Molecular Dynamics and Phase Transition in One-Dimensional Crystal of C$_{60}$ Encapsulated Inside Single Wall Carbon Nanotubes

E. Abou-Hamad,[†,#] Y. Kim,[‡,#] T. Wågberg,[§] D. Boesch,[⊥] S. Aloni,[⊥] A. Zettl,[⊥] A. Rubio,[‖] D. E. Luzzi,[‡,¶] and C. Goze-Bac[†,]*

[†]Laboratoire Colloïdes, Verres et Nanomatériaux, CNRS Université Montpellier 2, France, [‡]Department of Materials Science and Engineering, University of Pennsylvania, Philadelphia, Pennsylvania 19104, [§]Department of Physics, Umeå University, S-901 87 Umeå, Sweden, [⊥]Department of Physics, University of California at Berkeley, and Materials Sciences Division, Lawrence Berkeley National Laboratory, Berkeley, California, 94720, [‖]European Theoretical Spectroscopy Facility (ETSF), Dpto. Física de Materiales and Centro Mixto CSIC-UPV/EHU, Universidad del País Vasco UPV/EHU, Edificio Korta, Avd. Tolosa 72, 20018 San Sebastián, Spain, and [¶]Office of the Dean, Snell Engineering Research Center, Northeastern University, Boston, Massachusetts 02115. [#]Both authors contributed equally to this work.

ABSTRACT One-dimensional crystals of 25% ^{13}C-enriched C$_{60}$ encapsulated inside highly magnetically purified SWNTs were investigated by following the temperature dependence of the ^{13}C NMR line shapes and the relaxation rates from 300 K down to 5 K. High-resolution MAS techniques reveal that 32% of the encapsulated molecules, so-called the C$_{60}^{\alpha}$, are blocked at room temperature and 68%, labeled C$_{60}^{\beta}$, are shown to reversly undergo molecular reorientational dynamics. Contrary to previous NMR studies, spin—lattice relaxation time reveals a phase transition at 100 K associated with the changes in the nature of the C$_{60}^{\beta}$ dynamics. Above the transition, the C$_{60}^{\beta}$ exhibits continuous rotational diffusion; below the transition, C$_{60}^{\beta}$ executes uniaxial hindered rotations most likely along the nanotubes axis and freeze out below 25 K. The associated activation energies of these two dynamical regimes are measured to be 6 times lower than in fcc-C$_{60}$, suggesting a quiet smooth orientational dependence of the interaction between C$_{60}^{\beta}$ molecules and the inner surface of the nanotubes.

KEYWORDS: carbon nanostructures · dynamical properties · phase transition · nuclear magnetic resonance

© 2009 American Chemical Society

Among the various properties of single wall carbon nanotube (SWNT),[1−5] the quasi one-dimensional inner space they provide is unique. They are molecular cylinders of few nanometers in diameter and length that can be of the order of centimeters in length. Peapods being one-dimensional arrays of molecules inside SWNTs is the archetype of molecular engineering at the nanoscale.[6,7] Several interesting applications have been predicted in nanoelectronics, nanochemistry, and nanobiomedicine based on the physical properties of encapsulated molecules, which are expected to be different from those in bulk because of the one-dimensional confinement and the reduction in the number of nearest neighbor molecular structures.[8] Unfortunately, from an experimental point of view, little is known

about the real packing and dynamics of encapsulated species at this level. The discovery of confined fullerenes inside SWNTs by Luzzi and co-workers[6,7] initiated a launch of intensive efforts to study such properties in SWNTs. Peapods made of C$_{60}$ inside SWNTs have turned out to be a case study for such hybrid materials. The discovery of fullerenes in 1985 by Kroto *et al.* was followed by extensive studies of their electronic, optical, and biological properties.[9−16] Looking back, NMR investigations have played a major role in the understanding of the properties of fullerenes. In particular, the dynamical properties of the plastic crystalline phase of C$_{60}$ was elucidated by NMR.[12−15] C$_{60}$ molecules undergo molecular reorientational dynamics with temperature with a phase transition at 260 K. From 300 to 260 K, they are freely rotating in a face centered cubic (fcc) structure. From 260 to 100 K, their rotations are hindered and the structure transforms to simple cubic by orientational ordering.[12] In this temperature range, single or double bonds face the centers of pentagons or hexagons to maximize Coulomb attraction.[15] The hindered rotations stop below 85 K, where C$_{60}$ molecules finally freeze out.

With the recent success of the magnetic methods of purification of the SWNTs,[17,18] NMR spectroscopy is also expected to reveal its high potential in nanotube materials. In the present temperature dependence study, enabled by highly purified materials and high-resolution nuclear magnetic reso-
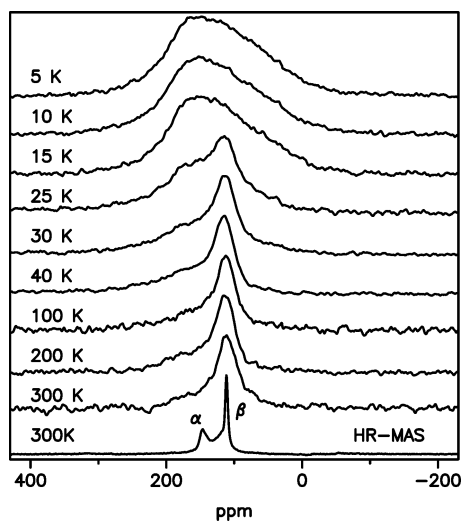
Figure 1. Static ^{13}C NMR spectra of C_{60} molecules encapsulated inside SWNTs at the indicated temperatures. Bottom spectrum: MAS ^{13}C NMR showing the isotropic lines of the C_{60}^{α} and C_{60}^{β}.

Figure 2. Simulated powder pattern line shape according to CSA tensor values described in the text for (a) SWNTs, (b) blocked C_{60}^{α}, (c) rotating C_{60}^{β}, and (d) the fit of the experimental spectrum (e) according to the indicated ratios.

nance, we investigate C_{60} encapsulated inside SWNTs which has been done partly by NMR[19−23] and inelastic neutron scattering[24] and the source of recent confusion. To clarify the debate, our experimental NMR work clearly reveals a strong modification due to one-dimensional confinement inside SWNTs of the molecular reorientational dynamics of C_{60} and the existence of a phase transition at 100 K.

RESULTS AND DISCUSSION

Figure 1 presents the high-resolution magic angle spinning ^{13}C NMR spectrum of the magnetically purified peapod samples at a spinning rate of about 10 kHz. Two sharp resonances labeled α at 148.2 ppm and β at 113.3 ppm are observed with ratios of 32 and 68%, repectively. According to the line positions and line widths, these resonances cannot be attributed to SWNTs or nonencapsulated C_{60} or polymerized phase of C_{60}. They can been interpreted in terms of C_{60}^{α} and C_{60}^{β}; the latter is diamagnetically shifted by −36.9 ppm from its normal position at 146.3 ppm by π electrons circulating on the SWNTs.[25] Therefore, the ^{13}C NMR spectra of peapods should be decomposed in three contributions: 16% SWNTs, 27% C_{60}^{α}, and 57% C_{60}^{β}. Figure 2 displays the static ^{13}C NMR spectrum at room temperature with its fit based on the sum of three powder patterns corresponding to SWNT, C_{60}^{α}, and C_{60}^{β}. In agreement with previous studies,[26] the following chemical shift anisotropy tensor principal values $\delta_{11}^{NT} = -42.2$ ppm, $\delta_{22}^{NT} = 164.8$ ppm, and $\delta_{33}^{NT} = 233.8$ ppm have been used for the SWNTs. The C_{60}^{α} components develop a line shape characteristic of a CSA powder pattern with CSA tensor principal values of $\delta_{11}^{\alpha} = 38.5$ ppm, $\delta_{22}^{\alpha} = 187.5$ ppm, and $\delta_{33}^{\alpha} = 218.5$ ppm. Figure 5 reveals that the second moment of C_{60}^{α} (solid
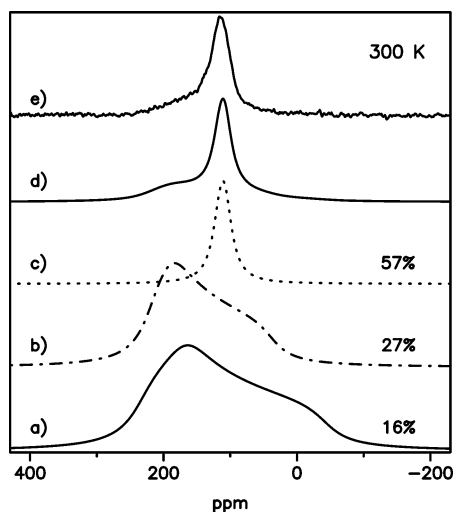
square) is constant from 300 K down to 5 K. This feature suggests that C_{60}^{α} is already blocked at room temperature. It has been pointed out that the cancellation of the diamagnetic shielding from the SWNT occurs in the vicinity of defects or holes in its side wall.[27,28] In addition, we suggest that these defects or holes freeze out also the rotational diffusion of C_{60}^{α} molecules through strong Coulombic interaction, with the energy barrier becoming too high. We turn to the case of the C_{60}^{β} resonance line, which is sharp, meaning that the C_{60}^{β} molecules are reorienting rapidly. The residual broadening of the line is attributed to the anisotropic diamagnetic shielding from the SWNTs.[25] An axially symmetric CSA tensor with principal values of $\delta_{11}^{\beta} = \delta_{22}^{\beta} = 106.9$ ppm and $\delta_{33}^{\beta} = 119.9$ ppm was obtained. Following our discussion above, the investigation of the molecular reorientational dynamics of C_{60} molecules encapsulated inside SWNTs should focus on the C_{60}^{β} contribution. Hence, our temperature dependence ^{13}C NMR study presented below is focused on the molecular reorientational dynamics of the C_{60}^{β} molecules.

Figure 1 shows static ^{13}C NMR spectra as a function of the temperature from 300 K down to 5 K. The sharp C_{60}^{β} at 111.3 ppm is observed from 300 K down to 30 K with no shift of the resonant frequency. Below 25 K, the line gradually broadens and develops a line shape characteristic of a chemical shift anisotropy powder pattern. At low temperature, the C_{60}^{β} presents a line shape characteristic of a CSA powder pattern with tensor principal values of $\delta_{11}^{\alpha} = 1.4$ ppm, $\delta_{22}^{\alpha} = 150.4$ ppm, and $\delta_{33}^{\alpha} = 181.4$ ppm. This feature indicates that, for most molecules, the rate of large amplitude molecular reorientation has become slow compared to the CSA width (3 kHz at 4.7 T). Above 25 K, large rotational motion of the
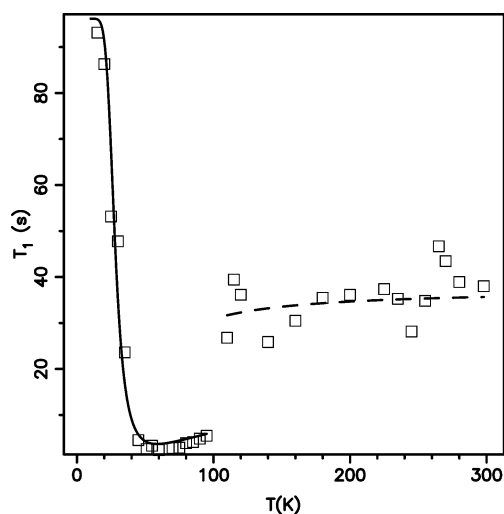
Figure 3. Spin−lattice relaxation time T_1 of C_{60}^β in peapods as a function of temperature. The phase transition occurs at $T_c = 100$ K. Note the abrupt change at T_c which occurs when C_{60}^β changes from continuous rotational diffusion (dashed line) to uniaxial rotation along the SWNT axis (solid line).

C_{60}^β molecules averages the CSA and results in the motional narrowing of the powder spectrum.[29]

The complete temperature dependence of the spin−lattice relaxation time T_1 is shown in Figure 3 and should be compared with experiments reported in ref 19. There is an obvious discrepancy between the two data sets around 100 K that should be clarified. These differences could originate from different types of SWNT samples. In particular, we report a discontinuity in the temperature dependence of T_1, which is expected if a phase transition occurs. In our experiments, the molecular reoriential motions that dominate the spin−lattice relaxation in C_{60} change abruptly at 100 K. In order to go further in our interpretation and to fit T_1 relaxation over the complete range of temperature, we use two different sets of parameters corresponding to above and below the phase transition temperature $T_c = 100$ K. The following contributions to the T_1 relaxation have been introduced:[29]

$$\frac{1}{T_1} = \frac{1}{T_{10}} + \frac{1}{T_{1M}} + \frac{1}{T_{1D}} \tag{1}$$

where $1/T_{10}$ is a temperature-independent constant background, $1/T_{1D}$ represents the contribution due to

fluctuating ^{13}C dipole−dipole interaction, and $1/T_{1M}$ is caused by fluctuating CSA; the latter two are due to molecular reorientation and depend on temperature. $1/T_{10}$ amounts in our case to 0.1 s^{-1}, which is quite small compared with other relaxation rates. It is most likely caused by paramagnetic impurities.

We discuss first the relaxation time T_{1M} caused by fluctuating local magnetic fields due to the reorientational motion of the C_{60}^β molecules. The CSA at the local ^{13}C site leads to a variation of the local field when the molecule reorients. The fluctuation $\Delta\omega_M$ will depend on the details of the isotropic and anisotropic molecular reorientations but will never exceed the total shift anisotropy. Since the details of the reorientations are not known, it will serve as an adjustable parameter. The corresponding spin−lattice relaxation rate can be readily expressed as[29−31]

$$\frac{1}{T_{1M}} = \frac{6}{40}\Delta\omega_M^2 \frac{2\tau}{1 + \omega_0^2\tau^2} \tag{2}$$

where ω_0 is the Larmor frequency. The relaxation rate is proportional to B_0^2 for $\omega_0\tau \ll 1$ and field independent for $\omega_0\tau \gg 1$, which explains the different behaviors at higher field reported in ref 19. A minimum in the relaxation time T_1 is expected according to Bloembergen, Purcell, and Pound[31] when $\omega_0\tau = 1$. The temperature dependence of the autocorrelation time τ follows an Arrhenius law:

$$\tau = \tau_0 \exp^{\Delta E_M/kT} \tag{3}$$

with an activation energy ΔE_M, reflecting the rotational barrier between different molecular orientations and τ_0 the autocorrelation time at infinite temperature.

Due to the isotope enrichment of our samples, we have to take into account the homonuclear dipolar couplings. This contribution is modeled by the additional term:[29]

$$\frac{1}{T_{1D}} = \frac{2}{3}\Delta\omega_D^2 \left(\frac{\tau}{1 + \omega_0^2\tau^2} + \frac{4\tau}{1 + 4\omega_0^2\tau^2} \right) \tag{4}$$

where $\Delta\omega_D$ represents the average fluctuations of the dipole−dipole interaction.

Equations 1−4 have been applied successfully to the fit of the spin−lattice relaxation times T_1 above and below T_c. Table 1 summarizes these two sets of fit-

TABLE 1. Reorientational Motion Parameters: Activation Energy ΔE, Autocorrelation Time τ_0, and Local Field Fluctuations $\Delta\omega$ Corresponding to T_1, T_2, and $\delta\nu$ in Peapods and fcc-C_{60} Fullerenes

experiment model	T_1 peapods $T_c = 100$ K	T_1 peapods $T_c = 100$ K	T_2 peapods $T_c = 100$ K	$\delta\nu$ peapods $T_c = 100$ K	T_1 fcc-C_{60}^{13} $T_c = 260$ K	T_1 fcc-C_{60}^{13} $T_c = 260$ K
temperature (K)	LT: 5 to 100	HT: 100 to 300	LT: 5 to 100	LT: 5 to 100	193 to 246	263 to 323
$\Delta\omega_M$ (s^{-1})	2π 2541	2π 3465	—	—	—	—
$\Delta\omega_D$ (s^{-1})	2π 475	—	—	—	—	—
$\Delta\omega_S$ (s^{-1})	—	—	2π 747	—	—	—
ΔE (meV)	27	8	28	35	250	42
τ_0 (s)	5×10^{-11}	5×10^{-11}	5×10^{-11}	5×10^{-11}	3×10^{-14}	5×10^{-12}

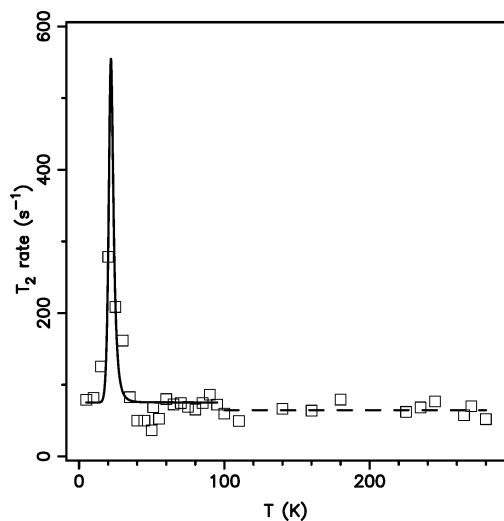**Figure 4. Spin−spin relaxation time T_2 of C_{60}^β in peapods as a function of temperature. The peak occurs when autocorrelation rate τ^{-1} is in the order of the line width (3 kHz at 4.7 T). Below 25 K, all the α and β C_{60} molecules are blocked.**

ting parameters corresponding to two different molecular reorientation regimes. The obtained values $\Delta\omega_M^{HT} = 2\pi\, 3465\ s^{-1}$ above T_c, $\Delta\omega_M^{LT} = 2\pi\, 2541\ s^{-1}$ and $\Delta\omega_D^{LT} = 2\pi\, 475\ s^{-1}$ below T_c are in reasonable agreement with the CSA line width at low temperatures (below 25 K). The activation energies $\Delta E_M^{HT} = 8$ meV and $\Delta E_M^{LT} = 27$ meV are estimated using an attempt autocorrelation time $\tau_0 = 5 \times 10^{-11}$ s.

We turn now to the discussion on spin−spin relaxation T_2, which is sensitive to fluctuating local fields on a time scale of about the line width (3 kHz in our case at 4.7 T). Figure 4 presents the $1/T_2$ relaxation rate from 300 K down to 5 K. A peak appears in $1/T_2$ around 25 K. In order to model the $1/T_2$ relaxation rate, we apply the following relation:[29,32]

$$\frac{1}{T_2} = \frac{1}{40}\Delta\omega_S^2\left(3\frac{2\tau}{1+\omega_0^2\tau^2} + 4\frac{2\tau}{1+\Delta\omega_S^2\tau^2}\right) \quad (5)$$

where $\Delta\omega_S$ corresponds to CSA fluctuations caused by reorientational process. The slow motion regime is observed when $\Delta\omega_S\tau \gg 1$ and the fast motional narrowing case for $\Delta\omega_S\tau \ll 1$. A peak in the $1/T_2$ relaxation rate is expected when $\Delta\omega_S\tau = 1$. Equation 5 has been applied to fit the experimental data below T_c as presented in Figure 4. The results are reported in Table 1. In agreement with T_1 relaxation, an activation energy of 28 meV was found. As expected above T_c, the $1/T_2$ relaxation rate is independent of temperature with a $T_2 \approx 11$ ms.

Figure 5 presents the second moment of the C_{60}^β line from 300 K down to 5 K. The motional narrowing around 25 K clearly indicates that the C_{60}^β rotational motion drastically changes at this temperature on a time scale of about 100 μs. The influence of rotational motion on the temperature-dependent line width can be described by the following implicit equation:[29]

$$(\delta_\nu)^2 = (\delta_\nu^{HT})^2 + (\Delta_\nu)^2\frac{2}{\pi}\arctan(\delta_\nu\tau) \quad (6)$$

where δ_ν^{HT} is the line width at high temperatures, Δ_ν the change in the line width from high to low temperatures. Using an autocorrelation time $\tau_0 = 5 \times 10^{-11}$ s, a self-consistent calculation gives an activation energy of 35 meV, in good agreement with previous estimations from T_1 and T_2 relaxation rates. Results are reported in Table 1.

Table 1 summarizes the reorientational motion parameters of one-dimensional encapsulated C_{60} fullerenes inside SWNTs. The parameters derived from the fits of T_1, T_2, and $\delta\nu$ are listed for comparison with the one from fcc-C_{60}.[13] Above $T_c = 100$ K, the measured temperature dependences T_1, T_2, and $\delta\nu$ clearly indicate fast reorientational dynamics of the C_{60} molecules. The relatively small value of the activation energy barrier (8 meV) suggests that the motion in the high-temperature phase approximates continuous rotational diffusion. Rotational diffusion would appear as orientational disorder in diffraction measurements. The dramatic change in kinetic parameters below 100 K reflects a drastic change in the nature of the molecular dynamics which could be explained by anisotropic uniaxial molecular rotations along the axis of the SWNTs. The activation energies below $T_c = 100$ K obtained from the fits of T_1, T_2, and $\delta\nu$ are 27, 28, and 35 meV, respectively. The differences are within the experimental error. The high rotational mobility of the C_{60} molecules is kept down to 25 K where it freezes out. These features suggest a smooth interaction between C_{60} and SWNTs.

Below T_c, an average value of 30 meV is almost one-eighth of the one admitted in fcc-C_{60} (250 meV). Above T_c, 8 meV is one-fifth of that in fcc-C_{60} (42 meV). Yildi-
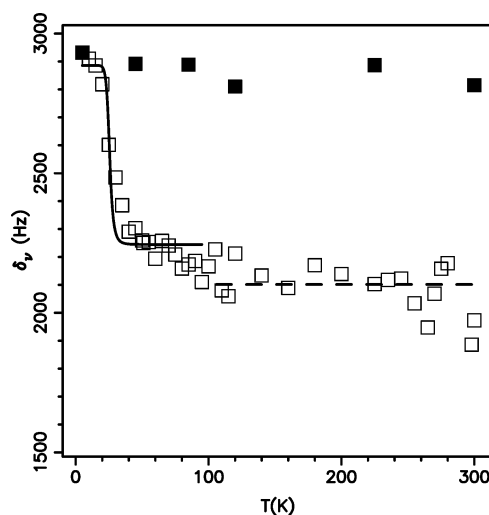

Figure 5. Second moment of the lines of the C_{60}^α (solid square) and C_{60}^β (open square). Note the small increase (200 Hz) at T_c from the continuous rotational diffusion (dashed line) to uniaxial rotational motion along the axis of the SWNTs (solid line). Below 25 K, the C_{60}^β molecules are blocked, which is evidenced by an increase of ≈800 Hz in δ_ν.

rim *et al.* predicted that, in fcc-C_{60},[15] a single or double bond in a fullerene prefers to face the center of a pentagon or a hexagon in neighboring fullerene to maximize Coulomb attraction.[33,34] Therefore, the activation energy for a rotation, which is a function of van der Waals interaction as well as the Coulomb attraction, would be as a first approximation, proportional to the number of nearest neighbors. The ratio of the number of nearest neighbors in peapods to that in fcc-C_{60} is one-sixth, which is consistent with the ratios of the activation energies mentioned above.

CONCLUSION

Reorientational motion of one-dimensional C_{60} array inside SWNTs has been investigated by ^{13}C NMR spectroscopy. The encapsulated fullerenes undergo a phase transition at T_c = 100 K (fcc-C_{60} at 260 K) from continuous rotational diffusion to uniaxial rotations and freeze out at 25 K (85 K in fcc-C_{60}). The significant changes in the dynamical properties of C_{60} encapsulated inside SWNTs result from the reduction of the number of nearest neighbors and its smooth interaction with the SWNT side walls.

METHODS

The 25% isotopically enriched ^{13}C fullerenes C_{60} were purchased from MER Corporation. As-received PII-SWNTs (diameter = 1.4 ± 0.2 nm) purchased from Carbon Solutions Inc. were purified with the novel magnetic filtration method as described in the literature.[17,18] The diamagnetic SWNT materials (30 mg) and ^{13}C-enriched fullerenes (20 mg) were outgassed in a dynamic vacuum 10^{-9} bar for 1 h at 650 and 300 °C, respectively. A quartz tube containing SWNTs and fullerene materials was sealed and annealed at 650 °C for 10 h in order for the fullerenes to fill the interiors of the SWNTs. After the filling step, the resulting peapod materials were post-annealed in a dynamic vacuum at 650 °C for 1 h to remove the non-encapsulated fullerenes. X-ray diffraction (XRD, Cu Kα with a wavelength of 1.54 Å) was used to probe the filling efficiency of the fullerenes into the SWNTs. The microstructures of peapods were examined using a JEOL 2010 transmission electron microscope at 80 keV to avoid electron beam damage. On the basis of TEM and XRD measurements, a minimum of 70% C_{60} filling ratio was found in our samples, in agreement with previous experiments.[18,19,24] Hence, taking into account the 25% ^{13}C isotope enrichment, a contribution of 16% from the SWNTs to the total ^{13}C NMR signal was estimated. Therefore, in our study, the observed ^{13}C NMR signal will clearly be dominated by the contribution of encapsulated C_{60} molecules. High-resolution ^{13}C magic angle spinning NMR experiments were carried out using Bruker ASX and Tecmag Apollo spectrometers at a static magnetic field of 4.7 T operating at Larmor frequencies of 50.3 MHz. Spectra were recorded by spin echo pulse sequence with four-phase alternation synchronized with the spinning rate for the MAS experiments. The spin−lattice relaxation time T_1 was measured by a conventional saturation−recovery pulse sequence with echo detection. The spin−spin relaxation time T_2 was measured by Carr−Purcell−Meiboom−Gill multiple echo pulse sequences. Temperature studies were performed in a sealed glass tube after being evacuated overnight at a secondary dynamic vacuum.

Supporting Information Available: Video 1: T > 100K, continous rotational diffusion of the C_{60} molecules inside SWNTs; video 2: 25K > T > 100K, uniaxial rotation of the C_{60} molecules inside SWNTs. Below 25K, the C_{60} molecules freeze out; video 3: Scenario at room temperature for the continous rotational diffusion of the C_{60} molecules inside SWNTs (68% β green) and blocked C_{60} molecules (32% α red) on a side wall defect. This material is available free of charge *via* the Internet at http://pubs.acs.org.

REFERENCES AND NOTES

1. Minot, E. D.; Yaish, Y.; Sazonova, V.; McEuen, P. L. Determination of Electron Orbital Magnetic Moments in Carbon Nanotubes. *Nature* **2004**, *428*, 536–539.
2. Itkis, M. E.; Niyogi, S.; Meng, M. E.; Hamon, M. A.; Hu, H.; Haddon, R. C. Spectroscopic Study of the Fermi Level Electronic Structure of Single-Walled Carbon Nanotubes. *Nano Lett.* **2002**, *2*, 155–159.
3. Saito, R.; Fujita, M.; Dresselhaus, G.; Dresselhaus, M. S. Electronic Structure of Chiral Graphene Tubules. *Appl. Phys. Lett.* **1992**, *60*, 2204–2007.
4. Ishii, H.; Kataura, H.; Shiozawa, H.; Yoshioka, H.; Otsubo, H.; Takayama, Y.; Miyahara, T.; Suzuki, S.; Achiba, Y.; Nakatake, M.; et al. Direct Observation of Tomonaga Luttinger Liquid State in Carbon Nanotubes at Low Temperatures. *Nature* **2003**, *426*, 540–544.
5. Javey, A.; Guo, J.; Wang, Q.; Lundstrom, M.; Dai, H. Ballistic Carbon Nanotube Field-Effect Transistors. *Nature* **2003**, *424*, 654–657.
6. Hornbaker, D. J.; Khang, S. J.; Misra, S.; Smith, B. W.; Johnson, A. T.; Mele, E. J.; Luzzi, D. E.; Yazdani, A. Mapping the One-Dimensional Electronic States of Nanotube Peapod Structures. *Science* **2002**, *295*, 828–831.
7. Smith, B. W.; Monthioux, M.; Luzzi, D. E. Encapsulated C_{60} in Carbon Nanotubes. *Nature* **1998**, *396*, 323–324.
8. Kolesnikov, A. I.; Zanotti, J. M.; Loong, C. K.; Thiyagarajan, P.; Moravsky, A.; Loutfy, R.; Burnham, C. Anomalously Soft Dynamics of Water in a Nanotube: A Revelation of Nanoscale Confinement. *Phys. Rev. Lett.* **2004**, *93*, 35503–35506.
9. Kroto, H. W.; Heath, J. R.; O'Brien, S. C.; Curl, R. F.; Smalley, R. E. C_{60}: Buckminsterfullerene. *Nature* **1985**, *318*, 162–163.
10. Dunne, L. J.; Sarkar, A. K.; Kroto, H. W.; Munn, J.; Kathirgamanathan, P.; Heinen, U.; Fernandez, J.; Hare, J.; Reid, D. G.; Clark, A. D. Electrical, Magnetic and Structural Characterization of Fullerene Soots. *J. Phys.: Condens. Matter* **1996**, *8*, 2127–2141.
11. Wilson, S. R. In *The Fullerene Handbook*; Kadish, K., Ruoff R., Eds.; Wiley: New York, 2000.
12. Heiney, P. A.; Fischer, J. E.; McGhie, A. R.; Romanow, W. J.; Denenstein, A. M.; McCauley, J. P.; Smith, A. B. Orientational Ordering Transition in Solid C_{60}. *Phys. Rev. Lett.* **1991**, *66*, 2911–2914.
13. Tycko, R.; Dabbagh, G.; Fleming, R. M.; Haddon, R. C.; Makhija, A. V.; Zahurak, S. M. Molecular Dynamics and the Phase Transition in Solid C_{60}. *Phys. Rev. Lett.* **1991**, *67*, 1886–1889.
14. Blinc, R.; Seliger, J.; Dolinsek, J.; Arcon, D. Two-Dimensional ^{13}C NMR Study of Orientational Ordering in Solid C_{60}. *Phys. Rev. B* **1994**, *49*, 4993–5002.
15. Yildirim, T.; Harris, A. B.; Erwin, S. C. Multipole Approach to Orientational Interactions in Solid C_{60}. *Phys. Rev. B* **1993**, *48*, 1888–1898.
16. Tycko, R.; Haddon, R. C.; Dabbagh, G.; Glarum, S. H.; Douglass, D. C.; Mujsce, A. M. Solid State Magnetic Resonance Spectroscopy of Fullerenes. *J. Phys. Chem.* **1991**, *95*, 518–520.

17. Kim, Y.; Luzzi, D. E. Purification of Pulsed Laser Synthesized Single Wall Carbon Nanotubes by Magnetic Filtration. *J. Phys. Chem. B* **2005**, *109*, 16636–16643.

18. Kim, Y.; Torrens, O. N.; Kikkawa, J. M.; Abou-Hamad, E.; Goze-Bac, C.; Luzzi, D. E. High Purity Diamagnetic Single Wall Carbon Nanotubes Buckypaper. *Chem. Mater.* **2007**, *19*, 2982–2986.

19. Matsuda, K.; Maniwa, Y.; Kataura, H. Highly Rotational C_{60} Dynamics Inside Single-Walled Carbon Nanotubes: NMR Observations. *Phys. Rev. B* **2008**, *77*, 75421–75426.

20. Zurek, E.; Pickard, C. J.; Autschbach, J. Density Functional Study of the ^{13}C NMR Chemical Shifts in Single Walled Carbon Nanotubes with Stone-Wales Defects. *J. Phys. Chem. C* **2008**, *112*, 11744–11750.

21. Besley, N. A.; Noble, A. NMR Chemical Shifts of Molecules Encapsulated in Single Walled Carbon Nanotubes. *J. Chem. Phys.* **2008**, *128*, 101102–101108.

22. Sebastiani, D.; Kudin, K. N. Electronic Response Properties of Carbon Nanotubes in Magnetic Fields. *ACS Nano* **2008**, *2*, 661–668.

23. Zurek, A.; Autschbach, J. NMR Computations for Carbon Nanotubes from First Principles: Present Status and Future Directions. *Int. J. Quantum Chem.* **2009**, *109*, 3343–3367.

24. Rols, S.; Cambedouzou, J.; Chorro, M.; Schober, H.; Agafonov, V.; Launois, P.; Davydov, V.; Rakhmanina, A. V.; Kataura, H.; Sauvajol, J. L. How Confinement Affects the Dynamics of C_{60} in Carbon Nanopeapods. *Phys. Rev. Lett.* **2008**, *101*, 065507–065510.

25. Marques, M.; d'Avezac, M.; Mauri, F. Magnetic Response and NMR Spectra of Carbon Nanotubes from *Ab Initio* Calculations. *Phys. Rev. B* **2006**, *73*, 125433–125438.

26. Goze-Bac, C.; Latil, S.; Lauginie, P.; Jourdain, V.; Conard, J.; Duclaux, L.; Rubio, A.; Bernier, P. Magnetic Interactions in Carbon Nanostructures. *Carbon* **2002**, *40*, 1825–1842.

27. Lopez-Urias, F.; Rodriguez-Manzo, J.; Munoz-Sandoval, E.; Terrones, M.; Terrones, H. Magnetic Responses in Finite Carbon Graphene Sheets and Nanotubes. *Opt. Mater.* **2006**, *29*, 110–115.

28. Abou-Hamad, E.; Kim, Y.; Talyzin, A. V.; Goze-Bac, C.; Luzzi, D. E.; Rubio, A.; Wagberg, T. Hydrogenation of C_{60} in Peapods: Physical Chemistry in Nano Vessels. *J. Phys. Chem. C* **2009**, *113*, 8583–8587.

29. Mehring, M. *Principles of High Resolution NMR in Solids*; Springer-Verlag: Berlin, Heidelberg, NY, 1983.

30. Abragam, A. *Principles of Nuclear Magnetism*; Oxford Science: New York, 1989.

31. Bloembergen, N.; Purcell, E. M.; Pound, R. V. Relaxation Effects in Nuclear Magnetic Resonance Absorption. *Phys. Rev.* **1948**, *73*, 679–712.

32. Rautter, J.; Grupp, A.; Mehring, M.; Alexander, J.; Mullen, K.; Huber, W. Electron Localization and Delocalization in Biselectrophores. *Mol. Phys.* **1992**, *76*, 37–45.

33. Girifalco, L. A.; Hodak, M.; Lee, R. S. Carbon Nanotubes, Buckyballs, Ropes, and a Universal Graphitic Potential. *Phys. Rev. B* **2000**, *62*, 13104–13110.

34. Hodak, M.; Girifalco, L. A. Systems of C_{60} Molecules Inside (10,10) and (15,15) Nanotube: A Monte Carlo Study. *Phys. Rev. B* **2003**, *68*, 085405–085411.